COMMUNICATION

Target-Specific 3D DNA Gatekeepers for Biomimetic Nanopores

*Wei Guo, Fan Hong, Nannan Liu, Jiayu Huang, Boya Wang, Ruixue Duan, Xiaoding Lou, and Fan Xia**

Stochastically opening and closing of the biological channels and pores on cell membrane is essential for the generation of nerve impulses, directionally uptake nutrients, and excrete metabolic wastes, maintaining fundamental life functions.[1] In the closed state, the channel current through these pore-forming membrane proteins shows zero in the mean suggesting that the biological membrane in this case is impermeable to any ionic species or natural substances. These adaptive ion channels and pores can be considered as the gatekeepers for living cells.[2] Inspired by the biological nanopores and their ability to manipulate the mass transportation on subcellular scale, the development of artificial, gate-like smart nanopores primarily for the fundamental research and applications of the surface-governed transport phenomena attracts broad interest in the interdisciplinary fields of materials science, chemistry, and nanotechnology.[3–5] For example, in the past decade, the design of biomimetic ionic diode and transistor devices with asymmetric ion transport properties is found to be crucial in building ionic circuit devices and energy conversion nanosystems.[6–9] However, being different from the biological channels, the leak of ionic current from the undesired region,[10–12] even in the closed state, becomes a challenge for the biomimetic nanopores that seriously reduced the sensitivity and resolution of the smart nanofluidic device in chemical sensing,[13–15] controlled released of drugs,[16–20] and energy-oriented applications.[21–25]

Recent advance in DNA bio-nanotechnology provides insights to solve the problem.[26–28] Owing to the unique material properties of DNA in molecular recognition and self-assembly, adaptable conformational transitions and high-dimensional nanostructures can be realized by designing the primary sequence of nucleotides.[29–33] For example, Siwy, Howorka, and co-workers. use protonatable AC-rich DNA oligomers to modify the tip region of a single conical polymer nanopore.[34] By lowering the pH to 5.5, the positively charged bases link the negative backbones, forming an electrostatic mesh in the nanopore that switches off the channel flux. One limitation of their device is the nanomechanical gating mechanism can only be applicable for nanopores with opening diameters less than 14 nm, due to the DNA oligomer they used contains merely 30 nucleotides. To further extend the application range of the DNA molecular gatekeepers, we adopt a more complex DNA structure, termed supersandwich, to self-assemble inside the solid-state nanopores.[35] High ON–OFF ratio of more than 10^2 can be found in large nanopores of about 200 nm in diameter.

Here, we report the use of three-dimensional (3D), cross-linked DNA superstructures as more efficient gatekeepers for solid-state nanopores. A hierarchical assembly strategy is adopted to construct the DNA structures into the nanopores (**Figure 1**). First, a sticky-ended, 3-point-star motif, termed Y-DNA, is presynthesized from three single-stranded DNAs (Y1, Y2, and Y3) through Waston–Crick base pairing (Figure S1, Supporting Information). Then, when the single-stranded capture probe (CP, 35-mer) modified nanopores are immersed in the solution containing Y-DNA and linker sequences (35-mer), the tiles of Y-DNA are further self-assembled and cross-linked into 3D superstructures via the hybridization of the free sticky ends with their complementary part on the CP or on the linker. The hybridization part in the two adjacent Y-DNAs contains 49 base pairs (Figure S1, Supporting Information), thus, the dihedral rotation between the two adjacent Y-DNAs is 1680.7° (not integral times of 180°), indicating the fact that the adjacent Y-DNAs cannot be placed in the same plane. Therefore, the as-formed DNA structures should extend to 3D space. Through a particular sequence design, the linker and CP contain embedded aptamer sequence for adenosine triphosphate (ATP, Table S1, Supporting Information). In the presence of ATP, the linker and CP change their conformation to bind the target with high binding affinity (the equilibrium dissociation constant (K_d) for ATP is 0.7×10^{-6}–8×10^{-6} M, depending on the salt and ionic concentration),[36] which consequently disassembles the 3D DNA nanostructures and reopens the pathway for ion conduction through the nanopores. The ON–OFF ratio between open and closed states approaches 10^3–10^5 and this gating mechanism can be applicable in nanopores with diameters up to ca. 650 nm, outperforming these low-dimensional or simple-structured DNA functional components. Interestingly, the DNA self-assembly induced closure process of the nanopores can be accelerated by nearly 2.8 times in a dilute mixture of organic solvent and aqueous buffer.

Gel electrophoresis is initially applied to confirm the formation of high-order DNA structures (Figure S2A, Supporting

Dr. W. Guo, F. Hong, N. Liu, J. Huang, B. Wang, R. Duan, Dr. X. Lou, Prof. F. Xia
Key Laboratory for Large-Format Battery Materials and Systems
Ministry of Education
School of Chemistry and Chemical Engineering
Huazhong University of Science and Technology
Wuhan 430074, P.R. China
E-mail: xiafan@hust.edu.cn
Dr. W. Guo
Laboratory of Bio-Inspired Smart Interface Science
Technical Institute of Physics and Chemistry
Chinese Academy of Sciences
Beijing 100190, P.R. China

DOI: 10.1002/adma.201405078

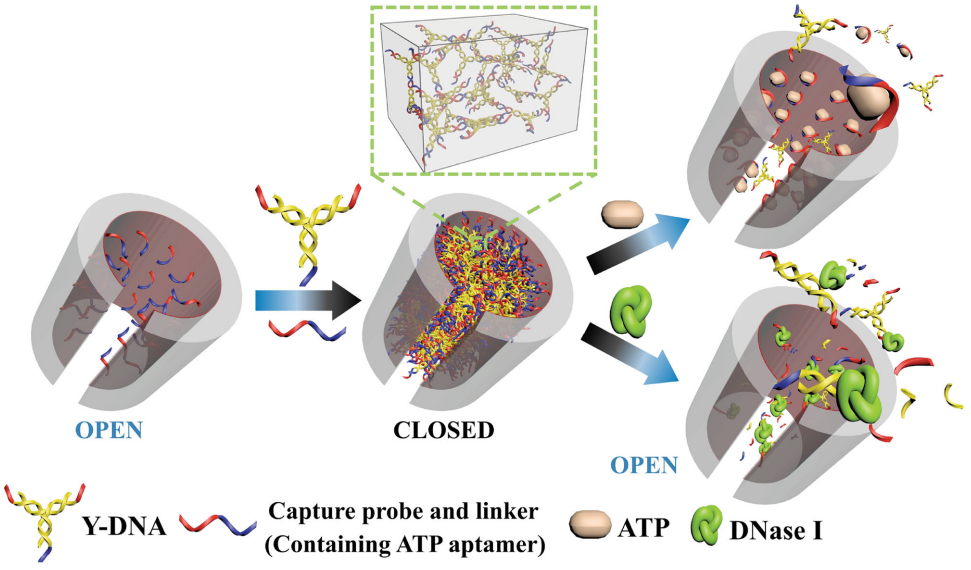

Figure 1. 3D, cross-linked DNA superstructures as efficient gatekeepers for solid-state nanopores. The nanopores are first modified with single-stranded capture DNA probes (the open state). In the presence of presynthesized Y-DNA and linker, the tiles of Y-DNA can be further assembled into 3D, cross-linked structures that efficiently block the pathway for ionic conduction (the closed state). The linker and capture probe contain aptamer sequence for ATP. Upon the ATP treatment, the cross-linked DNA superstructures are disassembled to reopen the nanopores (the open state). The use of DNase I to treat the DNA-blocked nanopores can similarly reopen the nanopores. In this case, the attached DNA moieties are digested by the DNase I, so that the nanopore gating system becomes invalid. This evidence justifies the ionic gating effect is induced by the DNA nanostructures.

Information). A ladder of different length of the DNA concatamers is observed after the mixture of Y-DNA and linker, the maximum of which approaches over 1500 bps. After the treatment of ATP, high-molecular-weight DNA concatamers that more than 400 bps are disassembled. We further examine the rheological properties of the proposed DNA structure (Figure S2B, Supporting Information). The shear-storage modulus (G′) is obviously higher than the shear-loss modulus (G″) over the entire frequency range, indicating that the DNA assemblies indeed form a cross-linked gel state in solution.

A cylindrical nanopore array in poly(ethylene terephthalate) (PET) membrane was prepared through first UV treatment and then chemical etching in 6 M NaOH solution at 50 °C (Figure S3, Supporting Information). The pore size can be controlled by the etching time. Then CP is immobilized onto the nanopore wall via a two-step chemical reaction (Figure S4, Supporting Information). The formation and elimination of the as-formed DNA nanostructures near the nanopore orifice can be observed with scanning electron microscope (SEM). After immersing the CP modified nanopores in the solution of Y-DNA (1×10^{-6} M) and linker (1.5×10^{-6} M), condensed DNA nanostructures are formed in the polymer nanopores (**Figure 2**B). In the presence of ATP (10×10^{-3} M), the DNA assemblies can be largely eliminated from the nanopores (Figure 2C). Using a FITC-labeled Y_2 sequence, laser scanning confocal microscope (LSCM) images on the cross-section of the nanopore membrane clearly show the DNA assembly inside the nanopores (Figure 2F). The width of the fluorescent region indicates the membrane thickness of about 12 µm. After the treatment with ATP, the fluorescent signals from inside the nanopores are substantially undermined by 68.0% (Figure 2G). These LSCM observations are in consistence with the results obtained from SEM and gel electrophoresis.

The formation of 3D, cross-linked DNA nanostructures in and out of nanopores efficiently switches off the transverse ionic flux, leading to a highly efficient nanofluidic gating

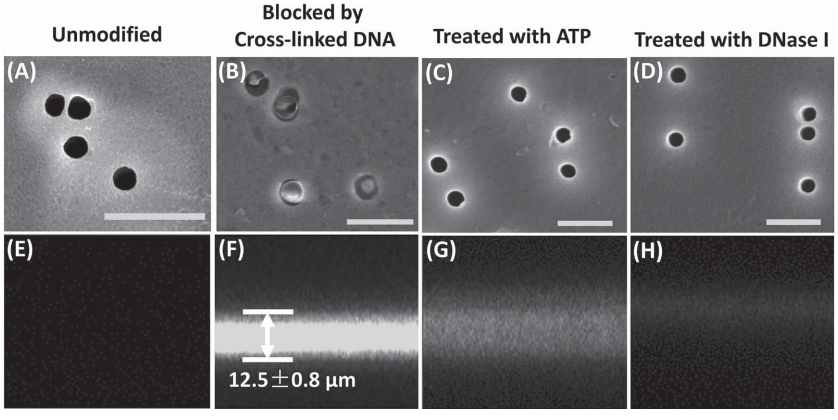

Figure 2. SEM and LSCM characterizations of the DNA assembly and disassembly on the orifice and inside the nanopores. The diameter of the unmodified nanopores is ca. 410 nm and no fluorescent signal is observed from the cross-section view under LSCM (A,E). After DNA assembly, the formation of DNA nanostructures near the pore orifice and inside the nanopore can be verified (B,F). The width of the fluorescent region in F) indicates the membrane thickness of about 12 µm. After treated with ATP, the DNA structures can be largely removed from the nanopores (C,G). When use DNase I to treat the DNA-modified nanopores, similar results can be obtained (D,H). The scale bars are 2 µm in A–D).

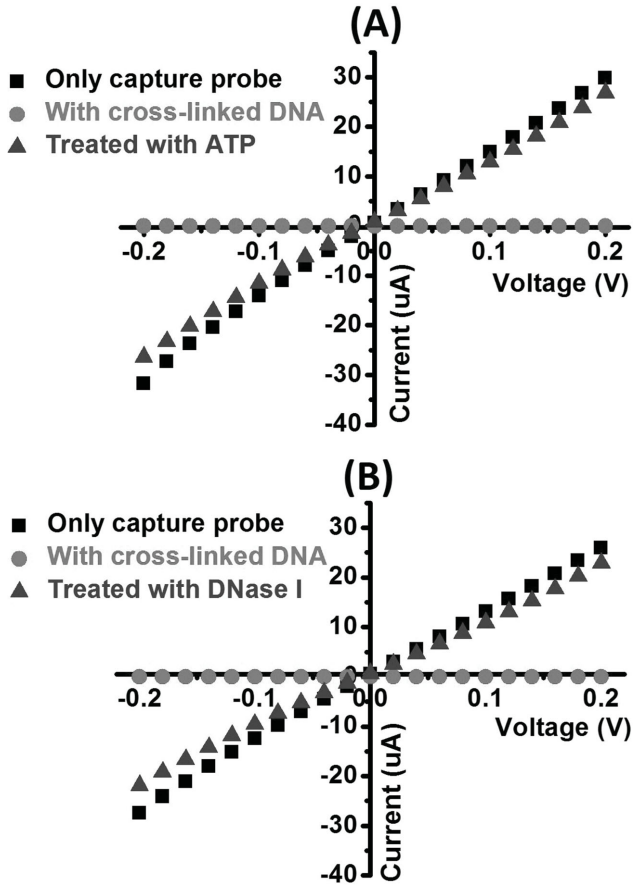

Figure 3. Highly effective nanofluidic gating system operated by the assembly of DNA superstructures and their disassembly by ATP. A) The assembly of 3D, cross-linked DNA structures remarkably inhibits the ion transport through the nanopores. The distinct contrast in the current–voltage responses before and after the DNA assembly shows an extremely high ON–OFF ratio of about 2000. Upon the treatment with ATP, the transmembrane ionic conductance retrieves to nearly 90% of that in its open state. B) The fully blocked ion transport can be similarly recovered upon the treatment with DNase I. In this case, the attached DNA moieties are digested by the DNase I and the device becomes invalid, which justifies the ionic gating effect is induced by the DNA nanostructures. The diameter of the unmodified nanopore is ca. 270 nm.

system. After modification with capture probes, the total transmembrane ionic conductance reduces ≈7.4% (Figure S5, Supporting Information). It is reasonable because the length of the capture probe (35-mer) is too short compared with the diameter of the nanopores (ca. 270 nm). After the self-assembly of the DNA superstructures, the resistance of the chemically modified nanopores remarkably increases from 7.27 kΩ (the open state) to 14.4 MΩ (the closed state, **Figure 3**A). The ON–OFF ratio approaches ca. 2000, indicating a highly effective electric seal in its closed state. After treated with ATP, these DNA fragments form loose structures and much of them can be washed out from the nanopores. Thus, they do not significantly impede the ion transport. Therefore, the transmembrane ionic conductance retrieves to ca. 89.0% of that measured in its open state. This switching process can be repeated by immersing the CP-modified nanopore membranes into the buffer solution containing Y-DNA and linker. We further justify the ionic gating behavior is induced by the DNA nanostructures. We use DNase I (0.5 U μL^{-1}) to treat the fully blocked nanopores (Figure 3B). The transmembrane ionic conductance also recovered to nearly 90% of that in the open state. But in this case, the DNase I treated nanopores cannot be reused for further test. This result is consistence with the SEM and LSCM characterizations that much of the attached DNA moieties, including the immobilized capture probes, have been digested and removed from in and outside the nanopore (Figure 2D,H).

Furthermore, we compare the gating performance of the 3D, cross-linked DNA superstructures with zero-dimensional (0D, hybridized DNA oligomers) and one-dimensional (1D, linear DNA concatamers containing repeated units of partially hybridized ssDNA) DNA structures in a series of nanopores with different pore size ranging from 270 to 650 nm (**Figure 4**A). Detailed sequence design can be found in Table S1, Supporting Information. For the hybridized DNA oligomers (0D), although the relatively short length can help to maintain persistence in the nanopores,[37] their length is too short with respect to the diameter of the wide nanopores of several hundred nanometers. Thus, the gating efficiency is extremely low (Figure 4B). The 1D DNA concatamer and the 3D cross-linked DNA structure show excellent gating performance. The ON–OFF ratio approaches more than one order of magnitude in the pore size ranging from 270 to 410 nm. Remarkably, the 3D, cross-linked DNA structure shows superior performance as a macromolecular gatekeeper. Its ON–OFF gating ratios maintain in the range of 10^3–10^5 in all the tested nanopores, especially in the wide nanopores up to 650 nm in diameter (Figures S6 and S7, Supporting Information), in which even the 1D DNA concatamers are almost invalid. We show three pieces of evidence to justify it is the formation of cross-linked Y-DNA that causes the blockade of nanopores. First, in our experiment, the monomer of Y-DNA is presynthesized in bulk solution, which is confirmed by gel electrophoresis (Figure S2A, Supporting Information). Second, the blockade events cannot be accomplished with the separate presence of Y-DNA monomers, or the linker strands (Figure S8, Supporting Information). Finally, the contribution of the linker DNA is also sequence-specific (Figure S9, Supporting Information). We conduct parallel DNA assembly experiment in nanopores using the linker sequence, mismatched linker sequence (containing 7 mismatched nucleotides), and a random sequence, respectively (Table S1, Supporting Information). The nearly perfect pore blockade events can be only found when using the right linker strands.

We suggest that there are two advantages in the more complex DNA structure: the dimension and the free sticky ends (Figure 4A). For the hybridized DNA oligomers, no free sticky ends exist for further growing of the short duplex structures, and thus, they can be approximately considered as "0D" DNA objects.[38,39] For the 1D DNA concatamer structures, in principle, one free sticky end always exists to prolong the duplex structure, leading to an improved gating property within wide nanopores. However, the prolonged duplex structure becomes flexible, for example, when it gets longer than 50 nm.[37] The isolated and flexible DNA concatamer tends to fall down inside the nanopores, resulting in higher steric hindrance that inhibits the duplex structures from further growth and leaves behind more voids for the leak of ionic current. For the 3D, cross-linked

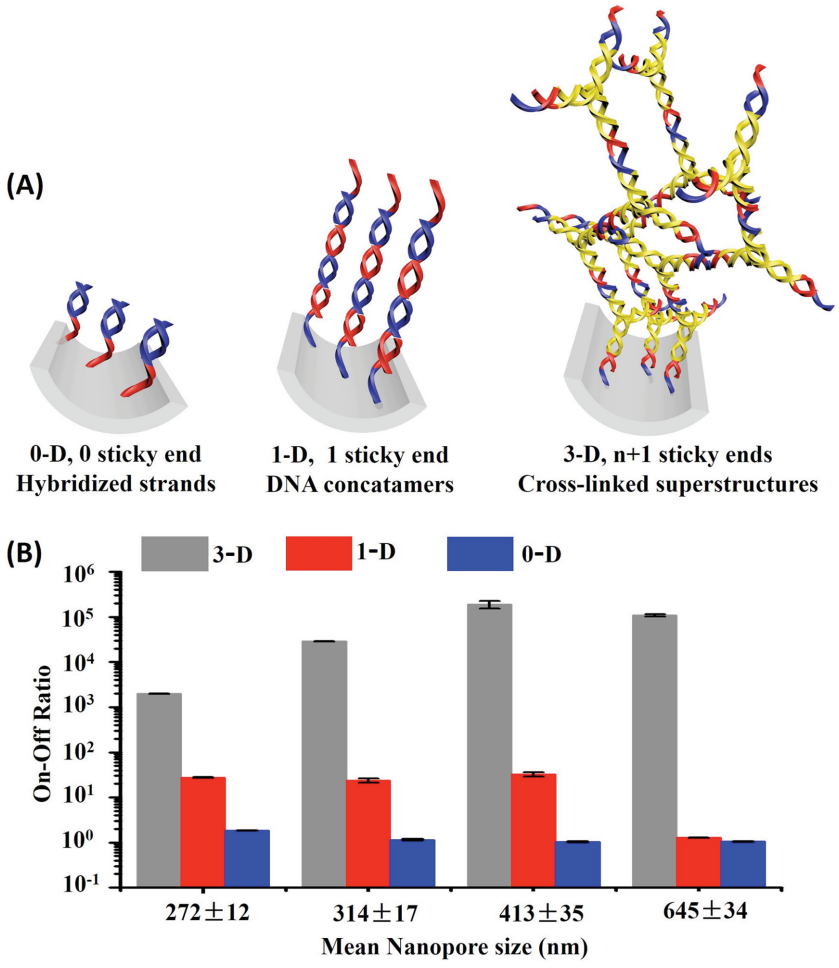

Figure 4. Comparison of the gating efficiency of three types of DNA structures. A), (left) hybridized DNA oligomers with no free sticky ends, considered as 0D DNA objects; (middle) 1D DNA concatamers with one free sticky end on each chain, composed of repeated units of partially hybridized ssDNA; (right) 3D cross-linked DNA structures containing *n*+1 free sticky ends (*n* is the number of Y-DNA unit). B) The 3D, cross-linked DNA structure shows superior performance to the 0D and 1D DNA structures. The ON–OFF ratios maintain 10^3–10^5 in all the tested nanopores with opening diameters ranging from 270 to 650 nm. The average pore size is the statistical results over one hundred pores. The deviations are given through five independent measurements.

structure, the amount of free sticky ends increase with the number of Y-DNA unit involved in the self-assembly process (*n*+1 free sticky ends are created when *n* units of Y-DNA are involved). This mechanism greatly improves the growing efficiency of the DNA assemblies and guides the growth of the DNA structure to 3D space. More importantly, the cross-linking effect between Y-DNA units initiated from different capture probes enhances the persistence of the DNA assemblies on the nanopore wall. Therefore, the 3D, bio-supramolecular gatekeepers outperform those low-dimensional DNA assemblies.

The assembly process of the DNA superstructure inside nanopores is studied by recording the leakage of ionic current during the closure of the nanopores. As shown in **Figure 5**, typically, the full closure time for the DNA-modified nanopores is about 1350 min in buffer solution. This time duration is much longer than that use of the 1D DNA concatamers to block the nanopore, which takes only about 500 min.[35] The structure of the 3D, cross-linked DNA assembly is much more complex than the 1D concatamer. Thus, it is reasonable that more time is needed to accomplish the self-assembly process. The relatively long closure time of more than 22 h have a negative impact on the reusability of the DNA-gated nanofluidic devices. In the following cycles, the nanopore devices show a remarkable decline in the gating efficiency. Several reasons may account for this phenomenon. First, the stability of the capture DNA decreased due to the long-time experiment.[40] In addition, after ATP treatment, there is still residual DNA probes persisted in the nanopores (see Figure 2G). This effect can be also reflected in the reduction in transmembrane ionic conductance. These warped DNA residuals may result in high steric hindrance that prevents the DNA assembly in the following cycles. In this case, 8 M urea can be used to treat the DNA modified nanopore membrane. After the modification of capture probe again, the DNA-gated nanofluidic device can be regenerated.

Interestingly, we discover that when 20% ethanol (volume ratio) was added in the buffer solution for DNA assembly, the closure process of the DNA-modified nanopores can be greatly accelerated (Figure 5). The full closure time is reduced to 480 min. From traditional perception, the presence of organic solvents, such as ethanol, denatures, and precipitates DNA, and consequently leads to slower and less stable hybridization. But, this principle may be only suitable for high-concentration of organic solvent. Smith and Liu have previously demonstrated that, if the volume fraction of alcohol is less than ≈30%, the alcohol leads to a faster DNA hybridization.[41] We have also proved that the presence of diluted ethanol does not influence the correct self-assembly of DNA chains, but the hybridization kinetics are remarkably accelerated in bulk solution and on electrode surface.[42] The acceleration mechanism is summarized as: first, the addition of ethanol decreases the activity of water, and consequently increases the effective concentration of DNA, resulting in faster hybridization rate.[41] Next, the activation energy of DNA hybridization is reduced by ethanol, which is favorable for increasing the reaction rate.[42] Finally, the addition of ethanol enhances the wetting properties of the nanopores embedded in PET membrane,[43,44] which could speed up the process of DNA tiles going inside the pore. The assembly of complex DNA structures into the nanopores is a very slow process because of the spatial restriction and the conformational hindrance. To the best of our knowledge, it is the first report that dilute organic solvent has an acceleration effect to the complex DNA assembly in nanopores.

In conclusion, we demonstrate a highly efficient nanofluidic switch gated by 3D, cross-linked DNA superstructures.

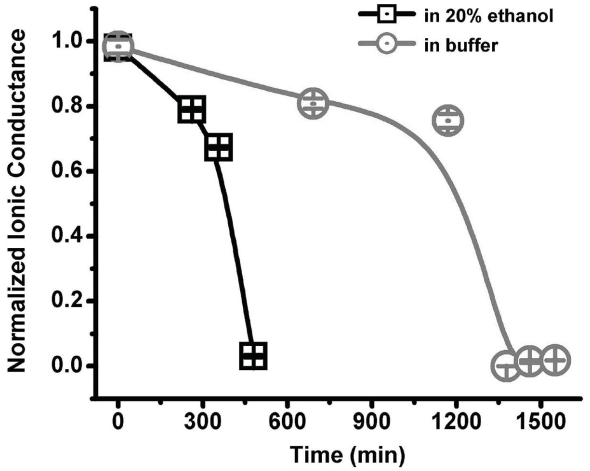

Figure 5. Accelerating the DNA self-assembly process inside nanopores. The assembly process of the DNA superstructures inside nanopores is monitored by recording the leak of ionic current in the open-to-closed process. In buffer solution, the full closure time for the DNA-modified nanopores is about 1350 min. By adding 20% ethanol, the full closure time can be greatly reduced to about 480 min.

The fully blocked nanopores can be reopened via target-specific ATP-aptamer interactions. Distinctly high ON–OFF ratios of about 10^3–10^5 can be found in nanopores with diameters up to ca. 650 nm. The 3D supramolecular gatekeepers outperform these low-dimensional or simple-structured DNA nanoactuators shown in Figure 4. Interestingly, the DNA assembly process inside nanopores can be speeded up by nearly 2.8 times with the addition of a small amount of ethanol into the buffer solution. Through a more elaborate sequence design, the well-established aptamer technology can be deeply integrated with the nanofluidic system to largely expand the range of the molecular targets from metal ions, small molecules, to biomacromolecules, and even for viruses, or cells. The DNA-regulated, all-or-none nanofluidic gating system anticipates potential for bioanalysis and smart nanofluidic devices with ultrahigh signal-to-noise ratio and accelerated response time.

Experimental Section

Nanopore Fabrication: Ion-tracked polyethylene terephthalate membranes (PET, 12 μm thick, 10^7 ions cm^{-2}) were pretreated by UV irradiation for 1 h on each side.[45] Then the PET membranes are chemically etched in 6 M NaOH solution at 50 °C to get cylindrical nanopores (Supporting Information). After etching, the PET membranes are thoroughly washed with and restored in pure water for at least 4 h before use.

Chemical Modification: To immobilize the capture DNA probe onto the wall of the nanopores, track-etched PET membranes are immersed in 600 μL solution containing 6 mg *N*-hydroxysulfosuccinimide (NHSS) and 30 mg 1-ethyl-3-(3-dimethylaminopropyl)carbodiimide (EDC) for 8 h to form NHSS esters. Then the PET-NHSS ester monolayers are reacted with a solution containing 5′-aminated capture DNA. 1×10^{-6} M 5′-aminated capture DNA is dissolved in 600 μL of 20×10^{-3} M Tris buffer (pH = 7.4, 100×10^{-3} M NaCl, 10×10^{-3} M $MgCl_2$) for 10 h. For the assembly of 3D DNA structures, the capture probe attached nanopores were immersed the in the solution containing Y-DNA (1×10^{-6} M) and linker (1.5×10^{-6} M). All the reactions are conducted at 4 °C. Detailed sequence can be found in Table S1, Supporting Information.

Gel Electrophoresis: The concentrations of Y-DNA and linker are 2×10^{-6} M and 3×10^{-6} M, respectively. They were reacted in separate vessels for 4 h in room temperature. For the disassembly of the DNA superstructure, ATP (10×10^{-6} M) and DNase I (150 U) are added to the DNA sample and reacted for 30 min at room temperature. 3% agarose gels containing 0.1 μL Gel-Red dye per milliliter are prepared using 1×TBE buffer. The gel electrophoresis is run at 90 V for 40 min.

Laser Scanning Confocal Microscopy (LSCM) Characterization: Fluorescein isothiocyanate labeled signal probes (Y2-FITC) were used for the LSCM observation (Nikon C1-si). The chemical modification strategy and the DNA assembly process are similar with that mentioned above.

Electrical Measurements: The sample membrane was mounted in between a custom-designed two-compartment electrochemical cell (Figure S11, Supporting Information).[46] The transmembrane ionic current was recorded with a picoammeter (Keithley 6487). A pair of Ag/AgCl electrodes was used to measure the resulting ionic current. Tris buffer solution was used as electrolyte. The effective membrane area for current recording is about 7 mm^2.

Supporting Information

Supporting Information is available from the Wiley Online Library or from the author.

Acknowledgements

W.G., F.H., and N.L. contributed equally to this work. This research is supported by National Research Fund for Fundamental Key Projects (2015CB932600, 2013CB933000 and 2011CB935700), National Natural Science Foundation of China (21375042, 21405054, 21103201, 11290163, and 91127025), 1000 Young Talent (to Fan Xia), and initiatory financial support from HUST. Wei Guo is supported by Beijing Nova Program.

Received: November 5, 2014
Revised: January 19, 2015
Published online: February 12, 2015

[1] E. Gouaux, R. MacKinnon, *Science* **2005**, *310*, 1461.
[2] B. Eisenberg, *Acc. Chem. Res.* **1998**, *31*, 117.
[3] C. Dekker, *Nat. Nanotechnol.* **2007**, *2*, 209.
[4] R. B. Schoch, J. Han, P. Renaud, *Rev. Mod. Phys.* **2008**, *80*, 839.
[5] W. Sparreboom, A. van den Berg, J. C. T. Eijkel, *Nat. Nanotechnol.* **2009**, *4*, 713.
[6] Z. S. Siwy, S. Howorka, *Chem. Soc. Rev.* **2010**, *39*, 1115.
[7] W. Guo, Y. Tian, L. Jiang, *Acc. Chem. Res.* **2013**, *46*, 2834.
[8] W. Guo, C. Cheng, Y. Wu, Y. Jiang, J. Gao, D. Li, L. Jiang, *Adv. Mater.* **2013**, *25*, 6064.
[9] W. Guo, L. Jiang, *Sci. China Mater.* **2014**, *57*, 2.
[10] A. R. Hall, A. Scott, D. Rotem, K. K. Mehta, H. Bayley, C. Dekker, *Nat. Nanotechnol.* **2010**, *5*, 874.
[11] R. Wei, T. G. Martin, U. Rant, H. Dietz, *Angew. Chem. Int. Ed.* **2012**, *51*, 4864.
[12] Y. Jiang, J. Gao, W. Guo, L. Jiang, *Chem. Commun.* **2014**, *50*, 14149.
[13] W. Guo, H. Xia, F. Xia, X. Hou, L. Cao, L. Wang, J. Xue, G. Zhang, Y. Song, D. Zhu, Y. Wang, L. Jiang, *ChemPhysChem* **2010**, *11*, 859.
[14] C. Plesa, A. N. Ananth, V. Linko, C. Gülcher, A. J. Katan, H. Dietz, C. Dekker, *ACS Nano* **2013**, *8*, 35.
[15] B. M. Venkatesan, R. Bashir, *Nat. Nanotechnol.* **2011**, *6*, 615.
[16] R. Casasús, E. Climent, M. D. Marcos, R. Martínez-Máñez, F. Sancenón, J. Soto, P. Amorós, J. Cano, E. Ruiz, *J. Am. Chem. Soc.* **2008**, *130*, 1903.
[17] W. Guo, H. Xia, L. Cao, F. Xia, S. Wang, G. Zhang, Y. Song, Y. Wang, L. Jiang, D. Zhu, *Adv. Funct. Mater.* **2010**, *20*, 3561.

[18] V. Cauda, H. Engelke, A. Sauer, D. Arcizet, C. Brauchle, J. Radler, T. Bein, *Nano Lett.* **2010**, *10*, 2484.
[19] C. L. Zhu, C.-H. Lu, X. Y. Song, H. H. Yang, X. R. Wang, *J. Am. Chem. Soc.* **2011**, *133*, 1278.
[20] L. Cao, W. Guo, Y. Wang, L. Jiang, *Langmuir* **2012**, *28*, 2194.
[21] W. Guo, L. X. Cao, J. C. Xia, F. Q. Nie, W. Ma, J. M. Xue, Y. L. Song, D. B. Zhu, Y. G. Wang, L. Jiang, *Adv. Funct. Mater.* **2010**, *20*, 1339.
[22] M. Ali, S. Mafe, P. Ramirez, R. Neumann, W. Ensinger, *Langmuir* **2009**, *25*, 11993.
[23] Y. Zhou, W. Guo, J. Cheng, Y. Liu, J. Li, L. Jiang, *Adv. Mater.* **2012**, *24*, 962.
[24] L. Cao, W. Guo, W. Ma, L. Wang, F. Xia, S. Wang, Y. Wang, L. Jiang, D. Zhu, *Energy Environ. Sci.* **2011**, *4*, 2259.
[25] J. Gao, W. Guo, D. Feng, H. Wang, D. Zhao, L. Jiang, *J. Am. Chem. Soc.* **2014**, *136*, 12265.
[26] O. I. Wilner, I. Willner, *Chem. Rev.* **2012**, *112*, 2528.
[27] B. Saccà, C. M. Niemeyer, *Angew. Chem. Int. Ed.* **2012**, *51*, 58.
[28] F. Zhang, J. Nangreave, Y. Liu, H. Yan, *J. Am. Chem. Soc.* **2014**, *136*, 11198.
[29] C. Zhang, Y. He, M. Su, S. H. Ko, T. Ye, Y. Leng, X. Sun, A. E. Ribbe, W. Jiang, C. Mao, *Faraday Discuss.* **2009**, *143*, 221.
[30] Y. Li, Y. D. Tseng, S. Y. Kwon, L. d'Espaux, J. S. Bunch, P. L. McEuen, D. Luo, *Nat. Mater.* **2004**, *3*, 38.
[31] C. C. Harrell, P. Kohli, Z. Siwy, C. R. Martin, *J. Am. Chem. Soc.* **2004**, *126*, 15646.
[32] F. Xia, W. Guo, Y. Mao, X. Hou, J. Xue, H. Xia, L. Wang, Y. Song, H. Ji, Q. Ouyang, Y. Wang, L. Jiang, *J. Am. Chem. Soc.* **2008**, *130*, 8345.
[33] V. Mussi, P. Fanzio, L. Repetto, G. Firpo, P. Scaruffi, S. Stigliani, G. P. Tonini, U. Valbusa, *Nanotechnology* **2010**, *21*, 145102.
[34] S. F. Buchsbaum, G. Nguyen, S. Howorka, Z. S. Siwy, *J. Am. Chem. Soc.* **2014**, *136*, 9902.
[35] Y. Jiang, N. Liu, W. Guo, F. Xia, L. Jiang, *J. Am. Chem. Soc.* **2012**, *134*, 15395.
[36] D. E. Huizenga, J. W. Szostak, *Biochemistry* **1995**, *34*, 656.
[37] H. Chang, F. Kosari, G. Andreadakis, M. A. Alam, G. Vasmatzis, R. Bashir, *Nano Lett.* **2004**, *4*, 1551.
[38] I. Vlassiouk, A. Krasnoslobodtsev, S. Smirnov, M. Germann, *Langmuir* **2004**, *20*, 9913.
[39] I. Vlassiouk, P. Takmakov, S. Smirnov, *Langmuir* **2005**, *21*, 4776.
[40] F. Xia, R. J. White, X. Zuo, A. Patterson, Y. Xiao, D. Kang, X. Gong, K. W. Plaxco, A. J. Heeger, *J. Am. Chem. Soc.* **2010**, *132*, 14346.
[41] B. D. Smith, J. Liu, *J. Am. Chem. Soc.* **2010**, *132*, 6300.
[42] D. Kang, R. Duan, Y. Tan, F. Hong, B. Wang, Z. Chen, S. Xu, X. Lou, W. Wei, B. Yurke, F. Xia, *Nanoscale* **2014**, *6*, 14153.
[43] W. Guo, J. Xue, L. Wang, Y. Wang, *Nucl. Instrum. Methods B* **2008**, *266*, 3095.
[44] M. R. Powell, L. Cleary, M. Davenport, K. J. Shea, Z. S. Siwy, *Nat. Nanotechnol.* **2011**, *6*, 798.
[45] N. Quoc Hung, A. Mubarak, B. Veronika, N. Reinhard, E. Wolfgang, *Nanotechnology* **2010**, *21*, 365701.
[46] N. Liu, Y. Jiang, Y. Zhou, F. Xia, W. Guo, L. Jiang, *Angew. Chem. Int. Ed.* **2013**, *52*, 2007.